

# Evolution of the superposition of displaced number states with the two-atom multiphoton Jaynes-Cummings model: interference and entanglement

Faisal A. A. El-Orany

Department of Mathematics and Computer Science, Faculty of Science, Suez Canal University, Ismailia, Egypt

**Abstract.** In this paper we study the evolution of the two two-level atoms interacting with a single-mode quantized radiation field, namely, two-atom multiphoton (, i.e.  $k$ th-photon) Jaynes-Cummings model when the radiation field and atoms are initially prepared in the superposition of displaced number states and excited atomic states, respectively. For this system we investigate the atomic inversion, Wigner function, phase distribution and entanglement. We show that there is a connection between all these quantities. Moreover, for symmetric (asymmetric) atoms the system can generate asymmetric (symmetric) cat states based on the values of the interaction parameters. This is shown in the behaviors of the Wigner function and phase distribution. The degree of entanglement for the field-atoms and the one-atom-remainder tangles depends on the energy follow between the bipartite. Also it is sensitive to the interference in phase space and the value of the parameter  $k$ .

PACS numbers: 42.50Dv, 42.60.Gd

## 1. Introduction

Entanglement is the striking feature of quantum mechanics revealing the existence of nonlocal correlations among different parts of a quantum system. A pair of quantum systems is called entangled if the measurement on one of them cannot be performed independent of that of the other. Quantum entanglement is a resource for certain tasks that can be performed faster or in a more secure way than the classical correlation. For these reasons entanglement plays an essential role in quantum information, e.g. quantum computing [1], teleportation [2], cryptographic [3], dense coding [4] and entanglement swapping [5]. These new aspects have launched intensive experimental efforts to generate entangled states and theoretical efforts to understand their structures. For instance, the

entanglement between two qubits in an arbitrary pure state has been quantified by the concurrence [6], however, that of the mixed states has been given as the infimum of the average concurrence over all possible pure state ensemble decomposition. The closed form for the concurrence has been expressed by Peres-Horodecki measure [7]. Moreover, this measure has been extended to include a bipartite system AB, with arbitrary dimensions  $D_A$  and  $D_B$  in an overall pure state [8]. The latter technique has been used to treat the entanglement for the tripartite quantum system in a Hilbert space with tensor product structure  $2 \otimes 2 \otimes \infty$  [9], e.g for the two-atom Tavis-Cummings model in an overall pure state.

The interaction between the radiation field and the two-level atom, namely, Jaynes-Cummings model (JCM) is an important topic in quantum optics since it is solvable in the framework of the rotating wave approximation (RWA) and it is experimentally implemented [10, 11]. Also the JCM is a rich source for the nonclassical effects, e.g. the revival-collapse phenomenon (RCP) in the evolution of the atomic inversion [12] and the generation of the cat states at one-half of the revival time [13, 14]. The importance of the JCM is increased as a result of the progress in the quantum information [15]. The JCM has been generalized and extended in different directions [16]. One of these directions, which is of particular interest, is the two two-level atoms interacting with a single quantized electromagnetic field (TJCM) [17, 18, 19, 20, 21]. The atomic inversion of the TJCM exhibits RCP having forms different from those of the JCM. This quantity has been investigated when the field is initially prepared in coherent state [17, 18, 19, 20], binomial state [21] and displaced squeezed state [22]. Also the entanglement for the TJCM when the field is initially prepared in coherent state [9] and binomial state [21] have been discussed, too.

The main object in quantum optics is to increase the nonclassical effects obtained from the quantum system. This has been achieved by developing new states beside the standard ones. One of these states is the displaced number state [23], which can be generated by passing coherent light through a non-linear medium [24]. In the framework of the superposition principle the superposition of displaced number states (SDN) has been developed as [25]:

$$\begin{aligned} |\alpha, m\rangle &= \lambda_\epsilon [\hat{D}(\alpha) + \epsilon \hat{D}(-\alpha)] |m\rangle \\ &= \sum_{n=0}^{\infty} C(n, m) |n\rangle, \end{aligned} \tag{1}$$

where  $\hat{D}(\alpha)$  is the displacement operator,  $\epsilon$  is a real parameter where its value will be specified in the text,  $\lambda_\epsilon$  is the normalization constant having the form:

$$\lambda_\epsilon^{-2} = 1 + \epsilon^2 + 2\epsilon \exp(-2\alpha^2) L_m(4\alpha^2) \tag{2}$$

and

$$C(n, m) = \lambda_\epsilon \langle n | [\hat{D}(\alpha) + \epsilon \hat{D}(-\alpha)] | m \rangle. \quad (3)$$

The photon-number distribution  $P(n)$  related to (1) is

$$P(n) = |C(n, m)|^2. \quad (4)$$

For particular values of the parameters the state (1) reduces to number states, coherent states, Schrödinger-cat states and displaced number state. The state (1) can be regarded as a single-mode vibration of electromagnetic field suddenly displaced by a collection of two displacements  $\pi$  out of phase with respect to each other. The generation of (1) has been established by the so-called "quantum state engineering" [25, 26]. Quite recently the decoherence for (1) in the framework of the standard master equation, which is described by the phase insensitive attenuators or amplifiers, has been investigated in [27]. Also the superposition of the  $N$  displaced number states [24] and superposition of the squeezed displaced number states [14, 28] have been developed, too. Finally, the density matrix  $\hat{\rho}$  of the superimposed states has two parts, namely, statistical-mixture part  $\hat{\rho}_S$  and interference part  $\hat{\rho}_I$ . The former provides information on the original components of the states and the latter gives the interference in phase space.

In the present paper we study the SDN against the two two-level atoms interacting with the quantized single-mode electromagnetic field (TJCM). In the RWA the Hamiltonian [17, 18, 19, 20, 21], which controls the system, takes the form

$$\begin{aligned} \frac{\hat{H}}{\hbar} &= \hat{H}_0 + \hat{H}_I, \\ \hat{H}_0 &= \omega \hat{a}^\dagger \hat{a} + \omega_a (\hat{\sigma}_1^z + \hat{\sigma}_2^z), \quad \hat{H}_I = \sum_{j=1}^2 \lambda_j (\hat{a}^k \hat{\sigma}_j^+ + \hat{a}^{\dagger k} \hat{\sigma}_j^-), \end{aligned} \quad (5)$$

where  $\hat{H}_0$  and  $\hat{H}_I$  are the free and interaction parts of the Hamiltonian,  $\hat{\sigma}_j^\pm$  and  $\hat{\sigma}_j^z$  are the Pauli spin operators of the  $j$ th atom;  $\hat{a}$  ( $\hat{a}^\dagger$ ) is the annihilation (creation) operator denoting the cavity mode,  $\omega$  and  $\omega_a$  are the frequencies of the cavity mode and the atomic systems (we consider that the two atoms have the same frequency),  $\lambda_j$  is the atom-field coupling constant of the  $j$ th atom and  $k$  is the transition parameter. In the paper we mainly deal with the ratio  $g = \lambda_2/\lambda_1$  and consider two cases, namely, symmetric and asymmetric according to  $g = 1$  and  $g \neq 1$ , respectively. Furthermore, we assume that  $\omega_a = 2k\omega$  (, i.e. the exact resonance case) and the two atoms and field are initially in the excited atomic states  $|+, +\rangle$  and the SDN, respectively. The atomic ground state is denoted by  $|-\rangle$ . Therefore, the dynamical state of the whole system can

be evaluated as:

$$\begin{aligned}
|\Psi(T)\rangle = \sum_{n=0}^{\infty} C(n, m) [X_1(T, n, k)|+, +, n\rangle + X_2(T, n, k)|+, -, n+k\rangle \\
+ X_3(T, n, k)|-, +, n+k\rangle + X_4(T, n, k)|-, -, n+2k\rangle],
\end{aligned} \tag{6}$$

where  $T = \lambda_1 t$  is the scaled time. The explicit forms for the dynamical coefficients  $X_j(T, n, k)$  can be found in [17, 18, 19, 20, 21], however, for analytical tasks we provide the forms of these coefficients for  $g = 1$ :

$$\begin{aligned}
X_1(T, n, k) &= \frac{n!(n+k)!}{[(n+k)!]^2 + n!(n+2k)!} \left[ \frac{(n+k)!}{n!} \cos(T\zeta_n) + \frac{(n+2k)!}{(n+k)!} \right], \\
X_2(T, n, k) &= X_3(T, n, k) = -i\sqrt{\frac{(n+k)!}{n!}} \frac{\sin(T\zeta_n)}{\zeta_n}, \\
X_4(T, n, k) &= \frac{(n+k)!\sqrt{n!(n+2k)!}}{[(n+k)!]^2 + n!(n+2k)!} [\cos(T\zeta_n) - 1],
\end{aligned} \tag{7}$$

where

$$\zeta_n = \sqrt{2\frac{(n+k)!}{n!} + 2\frac{(n+2k)!}{(n+k)!}}. \tag{8}$$

For this system we investigate the total atomic inversion  $\langle\sigma_z(T)\rangle = \frac{1}{2}[\langle\sigma_1^z(T)\rangle + \langle\sigma_2^z(T)\rangle]$ , Wigner ( $W$ ) function, phase distribution  $P(\Theta)$  and entanglement between different components of the system. The object of this study is as follows. There are some well-known phenomena occurred for the JCM so that we see the possible occurrence of such phenomena for the TJCM and what would be the influence of the interference in phase space on the behavior of the system. Also we quantify the entanglement between different components in the system. More illustratively, for JCM it has been shown that the Schrödinger-cat state can be generated at one-half of the revival time. Also this issue has been discussed only for the off-resonance TJCM when  $(k, g) = (1, 1)$  with  $\alpha \gg 1$  in the framework of  $Q$  function [29]. Here we investigate this behavior for the resonance TJCM the most general case, i.e. for all values of  $g$ , via  $W$  function, which gives better on quantum system than  $Q$  function. In this regard—for the system under consideration—we show that for the symmetric (asymmetric) case the asymmetric (symmetric) Schrödinger-cat states can be generated. This behavior likely occurs at the quarter of the revival time. Such generation of cat state is confirmed in the behavior of the  $P(\Theta)$ . Also we deduce the asymptotic form for the  $W$  function in the strong-intensity regime. Moreover, we shows that the degree of the entanglement is sensitive to the values of both  $k$ ,  $g$ , and  $\epsilon$ . Specifically, the degree of entanglement for the asymmetric case is greater than that of the symmetric one, and the interference in

phase space decreases the degree of entanglement. Finally, for  $k > 1$  the evolution of the tangles can be connected by the behavior of the corresponding atomic inversion.

The paper is organized in the following order: In section 2 we investigate the evolution of the  $\langle\sigma_z(T)\rangle$ ,  $W$  function and phase distribution. In section 3 we investigate the entanglement between different components of the system. In section 4 we summarize the main results.

## 2. Atomic inversion, Wigner function and phase distribution

One of the basic quantities related to the JCM is the atomic inversion, which represents the difference between the population of the excited and the ground atomic states. The evolution of the atomic inversion is representative by showing RCP. The occurrence of the RCP in this quantity has a quantum origin since it indicates the granular structure of the initial field distribution and also reveals the atom-field entanglement. A lot of efforts have been done for observing the RCP experimentally [10, 11, 30, 31, 32]. On the other hand, for the JCM it has been shown that there is a connection between the behaviors of the atomic inversion and both the  $W$  function and phase distribution. In this section we discuss this situation for the TJCM and compare the obtained results with those of the JCM. Also we investigate the influence of the interference in phase space on the behavior of the system.

We start with the total atomic inversion, which can be evaluated for (6) as

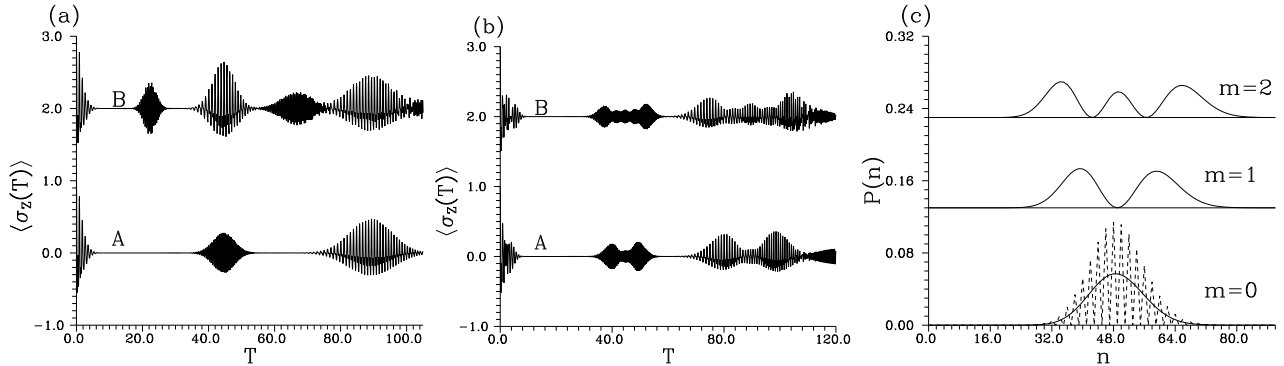


**Figure 1.** (a) and (b) represent the  $\langle\sigma_z(T)\rangle$  against the scaled time  $T$  for  $(\alpha, g) = (7, 0.5)$ , the curves  $A$  and  $B$  ( $\langle\sigma_z(T)\rangle + 2$ ) in (a) and (b) are given for  $(\epsilon, m) = (0, 0), (1, 0)$  and  $(0, 1), (0, 2)$ , respectively. (c)  $P(n)$  against  $n$  for  $(\epsilon, \alpha) = (0, 7)$  with the different values of  $m$  as indicated and shifted from bottom by 0, 0.1, 0.2. The dashed curve in (c) represents the  $P(n)$  of the  $(\epsilon, \alpha, m) = (1, 7, 0)$ .

$$\langle\sigma_z(T)\rangle = \sum_{n=0}^{\infty} |C(n, m)|^2 [|X_1(T, n, k)|^2 - |X_4(T, n, k)|^2]. \quad (9)$$

For the symmetric case and in the strong-intensity regime (SR), i.e.  $\alpha \gg 1$  and  $P(n)$  has a smooth envelope. The relation (9) reduces to

$$\langle \sigma_z(T) \rangle = \sum_{n=0}^{\infty} |C(n, m)|^2 \cos \left( 2T \sqrt{n + \frac{3}{2}} \right). \quad (10)$$

It is evident that this formula is quite similar to that of the standard JCM except the factor  $3/2$  has to be unity. Thus the behavior of the  $\langle \sigma_z(T) \rangle$  of the TJCM is quite similar to that of the JCM, i.e. the atomic inversion of the symmetric TJCM is insensitive of the existence of the other atom. In this case the revival time for  $(\epsilon, m) = (0, 0)$ , say, is  $T_r = 2\pi\sqrt{\bar{n} + 3/2}$ .

Now we draw the attention to the  $\langle \sigma_z(T) \rangle$  of the asymmetric case (see Figs. 1 for given values of the interaction parameters). Also we have plotted the corresponding initial  $P(n)$ . From this figure one can see that when  $P(n)$  exhibits multipeak structure, e.g.  $m \neq 0$ , the revival patterns in the corresponding  $\langle \sigma_z(T) \rangle$  are split. This is related to that each peak of  $P(n)$  provides its own RCP in the evolution of the  $\langle \sigma_z(T) \rangle$ , which interfere with those of the others to give such behavior. The comparison between the curves *A* and *B* in Fig. 1(a) shows that the revival time of the initial cat states is approximately one-half of that of the initial coherent states and the locations of the symmetric and asymmetric revival patterns in the two curves are quite different. This can be easily realized by noting that each  $\hat{\rho}_I$  and  $\hat{\rho}_S$  has its own RCP. Furthermore, the revival time of the former is the two times smaller than that of the latter. Therefore, when the revival patterns contributed by  $\hat{\rho}_I$  and  $\hat{\rho}_S$  occur at the same interaction time asymmetric patterns are exhibited in  $\langle \sigma_z(T) \rangle$ . This behavior is completely different from that of the symmetric case, which we have not presented.

As is well known that for the JCM the evolution of the  $W$  function [14] as well as the  $Q$  function [33, 34, 35, 36] provides information on the RCP in the  $\langle \sigma_z(T) \rangle$ . More illustratively, as the interaction is going on, the  $W$  function, which is initially presented by shifted Gaussian peak, splits into two peaks counter-rotate on a circle in the complex plane of the distribution with interference fringes in between. As the interaction proceeds the two peaks collide at the opposite end of the circle having the initial form, they split again, and so forth. In the framework of the  $\langle \sigma_z(T) \rangle$ : the collapse regions (revival patterns) in the Rabi oscillations occur in the course of the splitting (collision) of the distributions of the  $W$  function. In this regard, the Schrödinger-cat states are generated at the one-half of the revival time [14]. Also for the symmetric-off-resonance TJCM with the initial coherent light and using the  $Q$  function it has been numerically shown that asymmetric multipeak structure can be exhibited for  $\alpha \gg 1$  [29]. Moreover, the widths and the heights of these peaks can be controlled by the values of the detuning parameters and the type of the initial atomic states. In this part we investigate the evolution of the  $W$  function for the TJCM when  $\alpha$  is relatively small. This is inspired

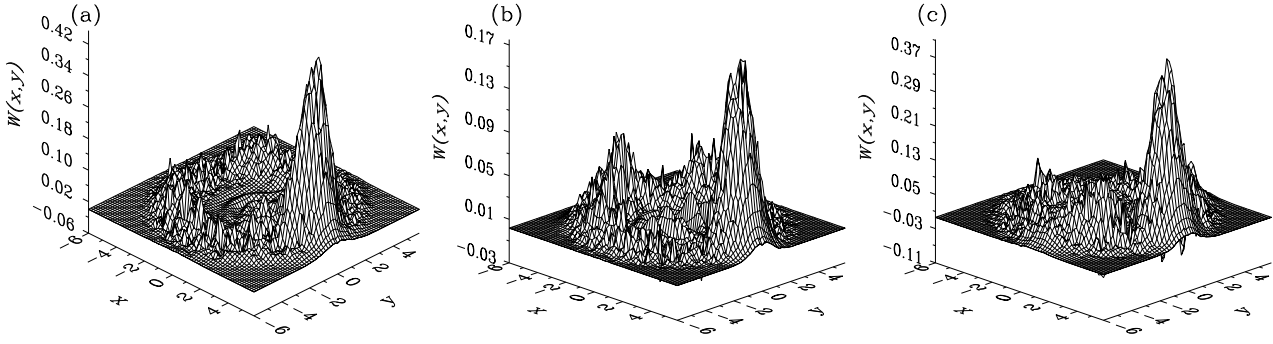


**Figure 2.** The  $W$  function against  $x$  and  $y$  for  $(g, \alpha, \epsilon) = (1, 3, 0)$ ,  $T = T_r$  (a),  $T_r/2$  (b) and  $T_r/4 \simeq 5.361749$  (c).  $T_r$  refers the revival time.

by the facts that the  $W$  function gives information on the quantum system better than  $Q$  function and the cat states generated for small  $\alpha$  are more nonclassical than those generated for strong initial intensity [37]. Additionally, we will deduce the asymptotic form for the state generated by the system when  $\alpha \gg 1$ . The  $W$  function for (6) can be easily evaluated as [14]:

$$W(x, y, T) = \frac{\exp(-|z|^2)}{\pi} \sum_{n, n'=0}^{\infty} C(n, m) C(n', m) (-1)^{n'} 2^{\frac{n-n'}{2}} z^{n-n'} \left\{ X_1(n, T) X_1(n', T) \sqrt{\frac{n!}{n'}} \right. \\ \times L_{n'}^{n-n'}(2|z|^2) + (-1)^k [X_2(n, T) X_2(n', T) + X_3(n, T) X_3(n', T)] \sqrt{\frac{(n'+k)!}{(n+k)!}} L_{n'+k}^{n-n'}(2|z|^2) \\ \left. + X_4(n, T) X_4(n', T) \sqrt{\frac{(n'+2k)!}{(n+2k)!}} L_{n'+2k}^{n-n'}(2|z|^2) \right\}, \quad (11)$$

where  $z = x + iy$  and  $L_n^\nu(\cdot)$  is the associated Laguerre polynomial. Generally, we have noted for small values of  $\alpha$  that the entanglement between the two atoms through the bosonic system leads to that the initial form of the  $W$  function cannot appear again after switching on the interaction. For instance, for the symmetric case the single-peak structure coming from the leading terms (cf. (7)) is dominant with distortion around circle in the  $xy$ -plane (see Figs. 2). In Figs. 2 the values of the interaction time have been chosen from the evolution of the corresponding  $\langle \sigma_z(T) \rangle$ . Comparison between Figs. 2(a), (b) and (c) shows that the nonclassicality (, i.e. the negativity) is more pronounced when  $T = T_r/4$ . Additionally, the negative values in  $W$  function at  $T = T_r$  is much greater than those at  $T = T_r/2$ , however, subsidiary peaks start to appear for the latter case. This will be remarkable in the behavior of the  $P(\Theta)$ , as we will see below.

Now we derive the asymptotic form for the  $W$  function for the case  $\alpha \gg 1$  and  $(g, k, \epsilon, m) = (1, 1, 0, 0)$  using SR. In this case we can replace  $C(n, 0)$  by  $C(n+1, 0)$  and  $C(n+2, 0)$  for the second and third terms in the curly brackets in (11), respectively, and then apply the SR for the arguments of the trigonometric functions. After some tricks,

using the generation function of the Laguerre polynomial and the Taylor expansion, the expression (11) can be evaluated as

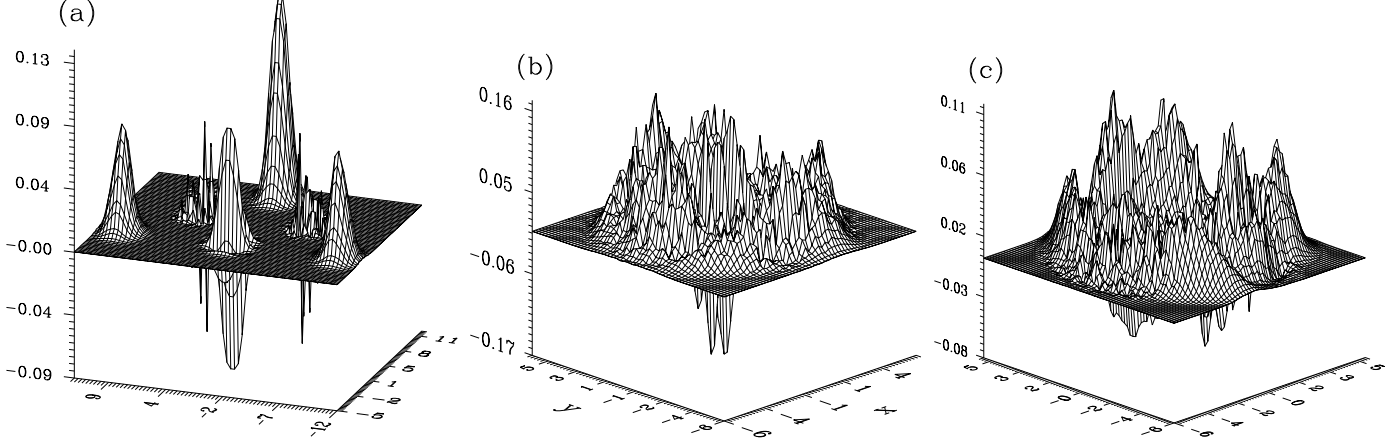


**Figure 3.** The  $W$  function against  $x$  and  $y$  for the asymptotic form (12) ( $\alpha, T$ ) =  $(7, T_r/4)$  (12) (a); the exact form (11) for  $(g, \alpha, \epsilon, T) = (0.5, 3, 0, 19.47003)$  (b) and  $(0.5, 3, 0, 10.18)$  (c).

$$W(x, y, T) \simeq \frac{1}{4\pi} \left\{ 2 \exp[-y^2 - (x - \sqrt{2}\alpha)^2] + \exp[-(x - \sqrt{2}\alpha \cos \eta)^2 - (y - \sqrt{2}\alpha \sin \eta)^2] \right. \\ \left. + \exp[-(x - \sqrt{2}\alpha \cos \eta)^2 - (y + \sqrt{2}\alpha \sin \eta)^2] - 2I_{int}(T) \sin \eta \right\}, \quad (12)$$

where  $\eta = \frac{T}{\sqrt{n}}$ , the interference part  $I_{int}(T)$  takes the form

$$I_{int}(T) = \exp[-(x - \sqrt{2}\alpha \cos \eta)^2 - y^2] \cos[2\eta' + 2\sqrt{2}x\alpha \sin \eta - \alpha^2 \sin(2\eta)] \sin \eta \\ + \exp[-(x - \sqrt{2}\alpha \cos^2 \frac{\eta}{2})^2] \left\{ \exp[-(y + \frac{\alpha}{\sqrt{2}} \sin \eta)^2] \sin \mu_+ \right. \\ \left. \exp[-(y - \frac{\alpha}{\sqrt{2}} \sin \eta)^2] \sin \mu_- \right\} \quad (13)$$

and

$$\mu_{\pm} = \eta' - \alpha^2 \sin \eta + \sqrt{2}\alpha(x \sin \eta \pm y \cos \eta) \pm \sqrt{2}\alpha y, \quad \eta' = T\sqrt{n} + \frac{T}{2\sqrt{n}}. \quad (14)$$

The formula (12) can give information on the  $W$  function for large values of  $\alpha$  for which it is difficult to deal with the exact form (11) because of the associated Laguerre polynomial. From (12) it is obvious that the first term is time independent since it is connecting with the leading terms in (7). Also  $W$  function includes three individual



peaks and three interference fringes each of them locating between two of these individual peaks. When  $\alpha$  is very large  $T_r \simeq 2\pi\sqrt{n}$  and we can extract various facts from (12). For instance, the interference part  $I_{int}(T)$  has no (maximum) contribution at  $T = T_r, T_r/2$  ( $T_r/4$ ). To be more specific, when  $T = T_r$  the  $W$  function reduces to that of the initial one, which is Gaussian bell centered at  $(\sqrt{2}\alpha, 0)$ , whereas at  $T = T_r/2$  the initial bell splits into two typical peaks localized at  $(\pm\sqrt{2}\alpha, 0)$  and eventually at  $T = T_r/4$  three-peak structure centered at  $(\sqrt{2}\alpha, 0), (0, \pm\sqrt{2}\alpha)$  with interference fringes in between are exhibited, i.e. three-component cat state is generated (see Fig. 3(a)). Moreover, we have checked the  $Q$  function for these values of the interaction times with  $\alpha \gg 1$  and obtained number of peaks as those exhibited for the  $W$  function. This behavior of the  $W$  function is different from that of the JCM even though the evolution of the atomic inversion for the two systems is quite similar. This can be easily understood by comparing the generalized Rabi oscillation for the JCM and the TJCM. Actually, for the symmetric case the Rabi oscillation of the TJCM is approximately two times greater than that of the JCM (cf. (8)). This fact explains why the cat states in the TJCM are generated at the quarter of the revival time, however, in the JCM at the one-half of the revival time. On the other hand, we have plotted the  $W$  function (11) for the asymmetric case in Figs. 3(b) and (c) for the revival and collapse times, respectively, when  $\alpha = 3$ . From these figures one can observe that the  $W$  function exhibits symmetric shapes in phase space, which are in contrast with the symmetric case (see Figs. 2). The nonclassical effects are more pronounced in the course of the revival time, which also are greater than those occurred for the symmetric case (compare Figs. 3(b) and (c) as well as Figs. 3 (b)-(c) and Figs. 2). Furthermore, the shapes presented in Figs. 3(b)-(c) indicate that the generated cat states are of the microscopic type. The  $W$  function of the microscopic cat state exhibits a complicated shape resulting from that the contribution of the different components of the state are located close to the phase-space origin. It is worth mentioning that the microscopic cat state (, i.e.  $\alpha$  is small) provides more nonclassical effects than the macroscopic one [38] (compare Figs. 3(a) and (b)).

Now we turn the attention to the phase distribution  $P(\Theta)$ . To investigate the  $P(\Theta)$  we use the Pegg-Barnett formalism [39], which for the density matrix elements  $\hat{\rho}_{n,n'}(T)$  gives

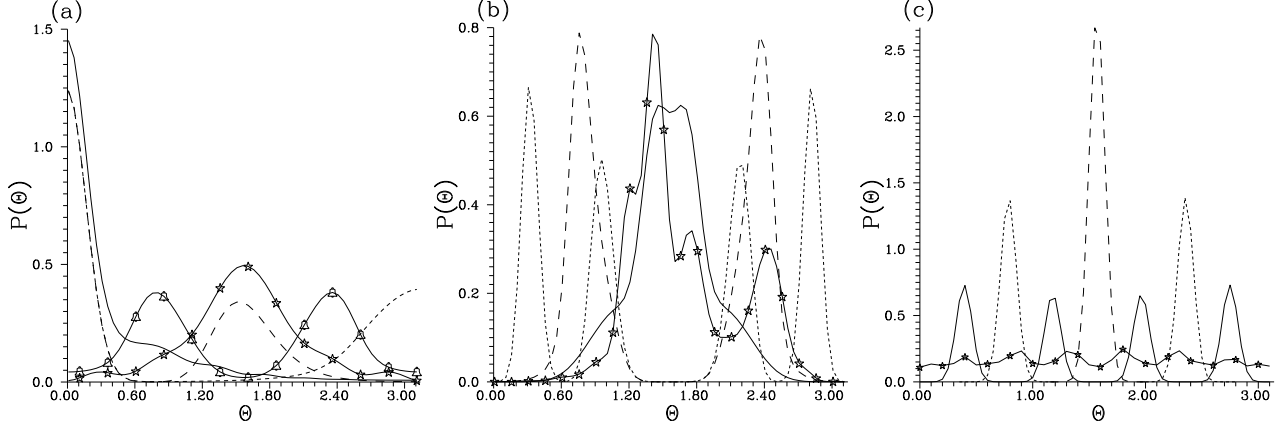


**Figure 4.** The phase distribution  $P(\Theta)$  against  $\Theta$ . Figure (a) is given for  $(\alpha, \epsilon, k) = (3, 0, 1)$  with  $(T, g) = (T_r, 1)$  (solid curve),  $(T_r/2, 1)$  (short-dashed curve),  $(T_r/4, 1)$  (long-dashed curve),  $(19.47003, 0.5)$  (star-centered curve) and  $(10.18, 0.5)$  (bell-centered curve). For (b)  $(\alpha, \epsilon, m, g, k) = (7, 1, 0, 0.5, 1)$  with  $T = 40.99995$  (second-revival time, solid curve),  $9.099998$  (collapse-time, short-dashed curve) and  $21.00004$  (first-revival-time, long-dashed curve). In (b) the star-centered curve is given for  $(\alpha, \epsilon, m, g, k, T) = (7, 0, 1, 0.5, 1, 41.04966)$ . For (c)  $(\alpha, \epsilon, m, g, k) = (7, 1, 0, 1, 2)$  for  $T = \pi/4$  (solid curve),  $\pi/2$  (short-dashed curve) and  $\pi$  (long-dashed curve). In (c) star-centered curve is given for  $(\alpha, \epsilon, m, g, k, T) = (7, 0, 0, 1, 3, \pi/4)$ .

$$\begin{aligned}
 P(\Theta) &= \frac{1}{2\pi} \left| \sum_{n, n'=0}^{\infty} \hat{\rho}_{n, n'}(T) \exp(i\Theta) \right|^2 \\
 &= \frac{1}{2\pi} \left\{ 1 + 2 \sum_{n > n'}^{\infty} C(n, m) C(n', m) [X_1(n, T) X_1(n', T) + X_2(n, T) X_2(n', T) \right. \\
 &\quad \left. + X_3(n, T) X_3(n', T) + X_4(n, T) X_4(n', T)] \cos[(n - n')\Theta] \right\},
 \end{aligned} \tag{15}$$

where we have considered that the phase reference  $\Theta_0 = 0$ . It is evident that  $P(\Theta) = P(-\Theta)$ . As a result of this symmetry we have plotted  $P(\Theta)$  against  $\Theta$  for  $0 \leq \Theta \leq \pi$  in Figs. 4(a)–(c) for given values of the interaction parameters. From Fig. 4(a), i.e. for the symmetric case, one can see that in the course of the revival time the  $P(\Theta)$  exhibits single-peak structure at  $\Theta = 0$ . This behavior is close to that of the initial coherent light. Nevertheless, at one-half (quarter) of the revival time two small lateral peaks (wings) occur. This indicates generation of the asymmetric cat states in the system. This behavior is not clear in the corresponding  $W$  function (see Figs. 2). It seems that the non-occurrence of the lateral peaks in the  $W$  function is related to that  $\alpha$  is considerably small. In this case the contribution of the different components in the  $W$  function will be close to the phase-space origin and destructively interfere with each

others. Furthermore, from the star-centered and bell-centered curves in Fig. 4(a) (, i.e. asymmetric case)  $P(\Theta)$  exhibits two-peak (four-peak) structure through the revival (collapse) time. In other words, two-component and four-component cat states can be generated in the asymmetric TJCM based on the values of the interaction parameters. This has been explained for the  $W$  function as a generation of microscopic cat states. Information on the interference in phase space is shown in Fig. 4(b) for the asymmetric case. For the asymmetric case there are two forms of the revival patterns: one is smooth and the other is asymmetric. Thus in Fig. 4(b) we have plotted the  $P(\Theta)$  for the first and second revival times. As is well known that for  $\Theta_0 = 0$  the  $P(\Theta)$  of the cat state possesses single-peak at  $\Theta = 0$  and two wings as  $\Theta \rightarrow \pm\pi$  [38]. This form changes by switching on the interaction where in the course of the collapse time asymmetric eight peaks are created, which are transformed to symmetric four peaks at the first revival time and eventually are collapsed to two-peak structure at the second revival time. It is obvious that the shape of the peaks in  $P(\Theta)$  includes information on the shape of the revival patterns, i.e. when the  $P(\Theta)$  exhibits smooth peaks the revival patterns are smooth and vice versa. Furthermore, the deformation in the  $P(n)$  leads to deformation in the peaks of  $P(\Theta)$  (see the star-centered curve in Fig. 4(b)). Also we have noted that when the values of the ratio  $g$  changes the number of peaks in  $P(\Theta)$  changes, too. Furthermore, we have noted that the behavior of the case  $k = 2$  is similar to that of  $k = 1$ , however, for the former the peaks are always smooth and narrower than those for the latter (see Fig. 4(c)). Also when  $k > 2$  the  $P(\Theta)$  exhibits multipeak structure (see the star-centered curve in Fig. 4(c)). This situation is similar to that of the two-mode JCM [40].

### 3. Entanglement

Entanglement is at the heart of quantum information theory. Various efforts are done to characterize qualitatively and quantitatively the entanglement properties of the quantum systems. This has been motivated by the progress in the experimental techniques aiming to create entangled states, which provide phenomena very different from the classical physics [41]. In this section we investigate the the entanglement for the system under consideration using the tangle  $I$  defined in [8]. Based on the symmetry exchange for the system we investigate two forms of tangles, which are field-atoms and one-atom-remainder. In other words, assume that  $f, A_1$  and  $A_2$  denoting the field, first atom and second atom, respectively. Therefore, the field-atoms tangle ( $f - A_1 A_2$ ) and one-atom-remainder tangle ( $A_1 - f A_2$ ), say, are define as [9]:

$$I_{f-A_1 A_2}(T) = 2[1 - \text{Tr} \hat{\rho}_f^2(T)] = 2[1 - \text{Tr} \hat{\rho}_{A_1 A_2}^2(T)], \quad (16)$$

$$I_{A_1-f A_2}(T) = 2[1 - \text{Tr} \hat{\rho}_{A_1}^2(T)] = 2[1 - \text{Tr} \hat{\rho}_{f A_2}^2(T)],$$

where, e.g.,  $\hat{\rho}_f(T)$  is the reduced density matrix of the field, which can be obtained by tracing the total density matrix of the system over a complete set of the atoms  $A_1A_2$ . The forms (16) quantify the degree of entanglement to which the ensembles behave as a collective entity. It is worth mentioning that the tangle here includes the notion of the purity. Generally, when  $I_{f-A_1A_2}(T) = 0$ , say, the parties  $f$  and  $A_1A_2$  are completely disentangled, but of course could be in states different from those of the initial ones. Nevertheless, when  $I_{f-A_1A_2}(T) = 2$  the parties are maximally entangled. In the following we use the terminologies:  $I_{f-A_1A_2}(T) \leq 1$  for weak entangled parties and  $I_{f-A_1A_2}(T) > 1$  for strong entangled parties.

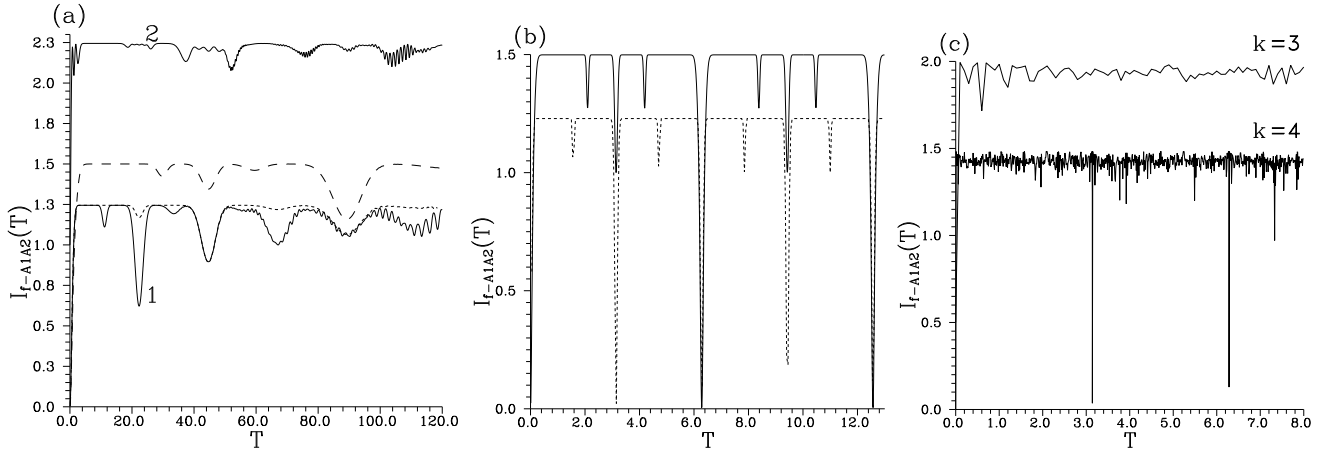


**Figure 5.** The tangle  $I_{f-A_1A_2}(T)$  against the scaled time  $T$  when  $\alpha = 7$  for (a)  $(\epsilon, g, m, k) = (0, 1, 0, 1)$  (the short-dashed curve),  $(0, 0.5, 0, 1)$  (the long-dashed curve),  $(1, 1, 0, 1)$  (the solid-curve-1) and  $(0, 0.5, 2, 1)$  (the solid-curve 2); (b)  $(\epsilon, g, m, k) = (0, 1, 0, 2)$  (short-dashed curve) and  $(0, 0.5, 0, 2)$  (solid curve); and (c)  $(\epsilon, g, m) = (0, 1, 0)$ . The solid-curve-2 in (a) is shifted by 1.

### 3.1. Field-atoms tangle

In this part we study the dynamical evolution for the tangle  $I_{f-A_1A_2}(T)$  for the system under consideration, which can be easily evaluated as

$$\begin{aligned}
 I_{f-A_1A_2}(T) = & 2 - 2 \sum_{n, n'=0}^{\infty} \left\{ C(n, m)C(n', m)X_1(n, T)X_1(n', T) + C(n - k, m)C(n' - k, m) \right. \\
 & \times [X_2(n - k, T)X_2(n' - k, T) + X_3(n - k, T)X_3(n' - k, T)] \\
 & \left. + C(n - 2k, m)C(n' - 2k, m)X_4(n - 2k, T)X_4(n' - 2k, T) \right\}^2.
 \end{aligned} \tag{17}$$

We have plotted (17) in Figs. 5(a)–(c) for different values of the interaction parameters. For all curves one can observe that at  $T = 0$ , where the bipartite is disentangled,

$I_{f-A_1A_2}(T) = 0$ . We start with the symmetric case in Fig. 5(a). From the short-dashed curve it is obvious that when  $t > 0$  the entanglement is established between the two parties and  $I_{f-A_1A_2}(T)$  goes rapidly to the strong-entangled region, stays for while, dips to weak entangled region and eventually becomes steady for large interaction time. This behavior is completely different from that of the purity of the JCM, which exhibits oscillatory behavior in a good correspondence with the revival patterns in the atomic inversion, and reduces to a pure state at the middle of the collapse time [14]. From the solid-curve-1 one can observe that the interference in phase space decreases the degree of entanglement at particular values of the interaction time and increases the oscillatory behavior in the tangle (compare the short-dashed curve and solid-curve-1). For the asymmetric case, i.e. the long-dashed curve and solid-curve-2, one can observe generally that the degree of entanglement becomes greater than that of the symmetric case (compare short-dashed and long-dashed curves). Also the influence of including Fock state in the optical cavity on the behavior of the  $I_{f-A_1A_2}(T)$  is shown by the solid-curve-2. From this curve it is obvious that the oscillatory behavior in  $I_{f-A_1A_2}(T)$  is increased compared to that of the initial coherent light, however, this behavior is not consistent with the RCP in the corresponding atomic inversion (see Fig. 1(b)). Now we draw the attention to Fig. 5(b) in which we have plotted  $I_{f-A_1A_2}(T)$  for the two-photon transition case, i.e.  $k = 2$ . This figure indicates that the bipartite can be periodically disentangled for the symmetric and asymmetric cases. For the symmetric case the  $I_{f-A_1A_2}(T)$  stays in the strong-entangled region most of the interaction time and goes to zero periodically with period  $\pi$ . This can be easily understood, e.g. for  $(\epsilon, g, m) = (0, 1, 0)$ , in the framework of the SR as follows. In this regime such terms  $1/n, 1/n^2, \dots$  tend to zeros leading to that  $\zeta_n \simeq 2(n + 5/2)$  (cf. (8)). Thus the state (6) can be expressed in the following asymptotic form:

$$\begin{aligned}
 |\Psi(T)\rangle \simeq \frac{1}{2} \sum_{n=0}^{\infty} C(n, 0) \{ & [\cos(2nT + 5T) + 1] |+, +, n\rangle - 2i \sin(2nT + 5T) \\
 & \times [|+, -, n+4\rangle + |-, +, n+2\rangle] + [\cos(2nT + 5T) - 1] |-, -, n+4\rangle \}.
 \end{aligned} \tag{18}$$

When  $T = s\pi$ ,  $s$  is odd number, the state (18) reduces to

$$|\Psi(T)\rangle \simeq \sum_{n=0}^{\infty} C(n, 0) |n+4\rangle \otimes \exp(i\pi) |-, -\rangle. \tag{19}$$

It is evident that in (19) the state of the radiation field is quite similar to that of the initial one but with four-photon shift. This behavior is similar to that of the purity of the JCM, but the forms of the phase factors and the number of shifted photons in the two quantities are different (compare (19) with (22)–(23) in [14]). Moreover, when  $T = s'\pi$  where  $s'$  is even integer, (18) reduces to its initial form. Also at  $T = \pi s''/2$ ,  $s''$

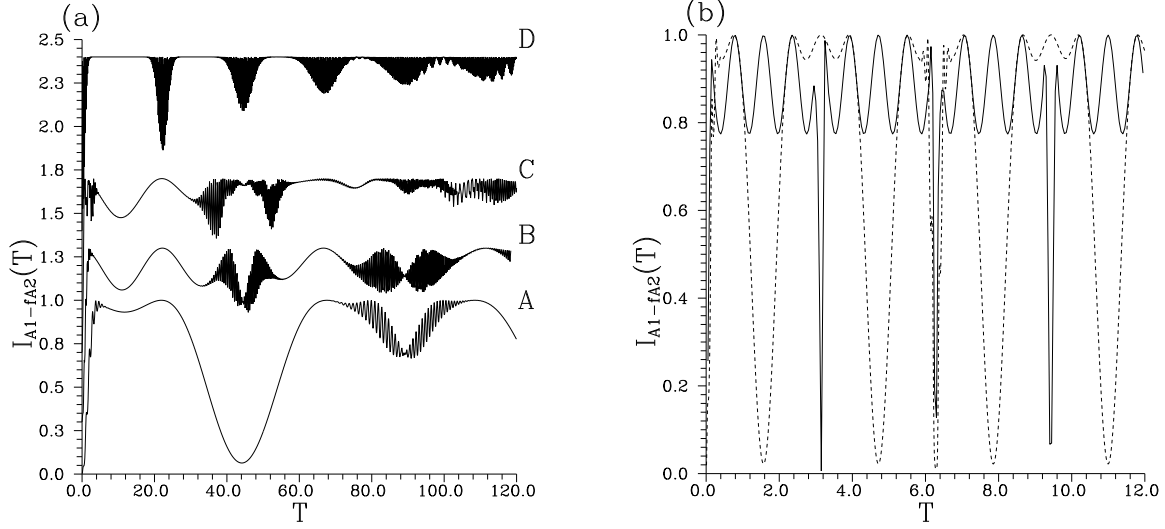


**Figure 6.** The  $I_{A_1-fA_2}(T)$  against the scaled time  $T$  when  $\alpha = 7$  for (a)  $(\epsilon, g, m, k) = (0, 0.5, 0, 1)$  (curve A),  $(0, 1, 0, 1)$  (curve B),  $(0, 0.5, 2, 1)$  (curve C) and  $(1, 1, 0, 1)$  (curve D), and (b)  $(\epsilon, g, m, k) = (0, 1, 0, 2)$  (solid curve) and  $(0, 0.5, 0, 2)$  (dashed-curve). In (a) the curves A–D are shifted from bottom by 0, 0.3, 0.7, 1.4, respectively.

is odd integer, the state (18) takes the form

$$\begin{aligned}
 |\Psi(T)\rangle \simeq \frac{1}{2} \sum_{n=0}^{\infty} C(n, 0) \{ & [|+, +, n\rangle - |-, -, n+4\rangle \\
 & - 2i(-1)^n [|+, -, n+2\rangle + |-, +, n+2\rangle]\}.
 \end{aligned} \tag{20}$$

For (20) one can easily prove that  $I_{f-A_1A_2}(T) = 1$ . All these analytical facts are remarkable in Fig. 5(b). For the asymmetric case, i.e. the solid curve in Fig. 5(b), we obtain behavior as that of the symmetric case but the degree of entanglement is greater and the disentanglement period is  $2\pi$ . Nevertheless, for this case it is difficult to obtain explicit forms for the state vector at  $I_{f-A_1A_2}(T) = 0$ . It is obvious that the disentanglement period depends on the value of the ratio  $g$ . Also the behavior of the  $I_{f-A_1A_2}(T)$  is consistent with the occurrence of the RCP in the evolution of the corresponding  $\langle\sigma^z(T)\rangle$ , we have checked this fact. From Fig. 5(c) one can see that for  $k = 3$  the bipartite are maximally entangled, however, for  $k = 4$  the degree of entanglement is decreased and the bipartite becomes periodically disentangled with period  $\pi$ . This behavior is similar that of the purity of the JCM. Finally, in Fig. 5(c) we have plotted  $I_{f-A_1A_2}(T)$  of the asymmetric case only where that of the symmetric case provides quite similar behaviors.

### 3.2. One-atom-remainder tangle

In this part we study the dynamical evolution for the tangle  $I_{A_1-fA_2}(T)$ , which can be expressed as:

$$\begin{aligned}
I_{A_1-fA_2}(T) = & 2 - 2 \sum_{n,n'=0}^{\infty} \left\{ |C(n,m)C(n',m)|^2 [|X_1(n,T)|^2 + |X_3(n,T)|^2] [|X_1(n',T)|^2 + |X_3(n',T)|^2] \right. \\
& + |C(n,m)C(n',m)|^2 [|X_2(n,T)|^2 + |X_4(n,T)|^2] [|X_2(n',T)|^2 + |X_4(n',T)|^2] \\
& + 2C(n+k,m)C(n,m)C(n'+k,m)C(n',m) [X_1(n+k,T)X_2^*(n,T) + X_3(n+k,T)X_4(n,T)] \\
& \left. \times [X_1(n'+k,T)X_2^*(n',T) + X_3(n'+k,T)X_4(n',T)] \right\}.
\end{aligned} \tag{21}$$

We have plotted  $I_{A_1-fA_2}(T)$  in Figs. 6 for the given values of the interaction parameters. The obvious remark from these figures is that  $0 \leq I_{A_1-fA_2}(T) \leq 1$ . This is completely different from the behavior of the  $I_{f-A_1A_2}(T)$  (compare Figs. 5 and 6 as well as expressions (17) and (21)). This indicates that the degree of entanglement for the one-atom-remainder tangle is less than that of the field-atoms tangle. Also this shows that the quantum entanglement cannot be equally distributed among many different objects. This can be explained as follows. We have an isolated system, i.e. the interaction with the environment is neglected, and hence the energy in the field and the two-atom system is periodically exchanged. In other words, when the  $k$  photons are annihilated from the radiation field they are created, i.e. equally distributed, in the two-atom party and vice versa. This means that the energy included in the  $fA_2$  party is more than that in the  $A_1$  party. Actually, the entanglement is a direct consequence of the energy follow between the two parties. The rate of follow of energy in the bipartite of the  $I_{f-A_1A_2}(T)$  is greater than that in the  $I_{A_1-fA_2}(T)$  and this could be the origin in the difference between the evolution of the two tangles. Now from the curves B and D in Fig. 6(a), i.e. symmetric case, one can observe that in contrast to  $I_{f-A_1A_2}(T)$  the  $I_{A_1-fA_2}(T)$  exhibits an oscillatory behavior in a good correspondence with the revival patterns in  $\langle \sigma_z(T) \rangle$ . Also the interference in phase space decreases the degree of entanglement in the  $I_{A_1-fA_2}(T)$  (compare curves B and D). It is worth mentioning that the curve D is quite similar to that of the purity of the JCM (see Fig. 2 in [42]). For the asymmetric case, and from the curve A one can observe that  $I_{A_1-fA_2}(T)$  exhibits compound behavior, i.e. it includes periodic and oscillatory behaviors. Also the bipartite can be approximately disentangled in the course of the first revival pattern. As in  $I_{f-A_1A_2}(T)$  the Fock state increases the range of the oscillatory behavior in the  $I_{A_1-fA_2}(T)$  (see the curve C). From Fig. 6(b), which is given for the case  $k = 2$ , one can see that for the symmetric case the  $I_{A_1-fA_2}(T)$  exhibits disentanglement periodically with period  $\pi$  (cf. (19)) as in  $I_{f-A_1A_2}(T)$  and also includes oscillatory behavior. The  $I_{A_1-fA_2}(T)$  of the

asymmetric case (, i.e. dashed curve) provides two types of disentanglement long lived (at  $T = \pi/2, 3\pi/2$ ) and instantaneous (at  $T = 2\pi$ ) and they occur periodically with period  $2\pi$ . For the cases  $k = 3, 4$  we have noted that the  $I_{A_1-fA_2}(T) \simeq 1$  with periodic disentanglement only for the case  $k = 4$ .

#### 4. Conclusion

In this paper we have treated the system of two two-level atoms interacting with multiphoton single-mode field. The two atoms and the field are initially prepared in the excited atomic states and in the superposition of displaced number states, respectively. We have investigated the behavior of the atomic inversion,  $W$  function, phase distribution and entanglement. We have shown that the TJCM can generate asymmetric (symmetric) cat states at quarter of the revival time for the symmetric (asymmetric) case. Also this has been confirmed in the behavior of the phase distribution. Moreover, we have deduced the asymptotic form for the  $W$  function when  $\alpha \gg 1$ . Also we have noted that when the values of  $g$  changes the number of the components of the generated cat state in the system changes, too. The  $P(\Theta)$  exhibits multipeak structure for  $k > 2$ . For the entanglement we have investigated two types, namely, field-atoms and one-atom-remainder tangles. We have shown that the degree of entanglement in  $I_{f-A_1A_2}$  is much greater than that in  $I_{A_1-fA_2}$ . We have explained this in the framework of the rate of energy flow between different parties of the system. We have obtained the following facts related to entanglement. The degree of entanglement for the asymmetric case is greater than that of the symmetric one. The interference in phase space decreases the degree of entanglement. There is a similarity between the dynamical behavior of the  $I_{f-A_1A_2}(T)$  and the purity of the JCM only for  $k > 1$ .

#### Acknowledgments

I would like to thank the Abdus Salam International Centre for Theoretical Physics, Strada Costiera, 11 34014 Trieste Italy for the hospitality and financial support under the system of associateship, where a part of this work is done.

#### References

- [1] Benenti G, Casati G and Strini G 2005 "Principle of Quantum Computation and Information" (World Scientific, Singapore).
- [2] Bennet C H, Brassard G, Crepeau C, Jozsa R, Peres A and Wootters W K 1993 *Phys. Rev. Lett.* **70** 1895.
- [3] Ekert A 1991 *Phys. Rev. Lett.* **67** 661; Cirac J I and Gisin N 1997 *Phys. Lett. A* **229** 1; Fuchs C A, Gisin N, Griffiths R B, Niu C-S and Peres A 1997 *Phys. Rev. A* **56** 1163.



- [4] Ye L and Guo G-C 2005 *Phys. Rev. A* **71** 034304; Mozes S, Oppenheim J and Reznik B 2005 *Phys. Rev. A* **71** 012311.
- [5] Glöckl O, Lorenz S, Marquardt C, Heersink J, Brownnutt M, Silberhorn C, Pan Q, Loock P V, Korolkova N and Leuchs G 2003 *Phys. Rev. A* **68** 012319; Yang M, Song W and Cao Z-L 2005 *Phys. Rev. A* **71** 034312; Li H-R, Li F-L, Yang Y and Zhang Q 2005 *Phys. Rev. A* **71** 022314.
- [6] Wootters W K 1998 *Phys. Rev. Lett.* **80** 2245; Hill S and Wootters W K 1997 *Phys. Rev. Lett.* **78** 5022.
- [7] Peres A 1996 *Phys. Rev. Lett.* **77** 1413; Horodecki P 1997 *Phys. Lett. A* **232** 333.
- [8] Rungta P, Bužek V, Caves C M, Hillery H and Milburn G J 2001 *Phys. Rev. A* **64** 042315.
- [9] Tessier T E, Deutsch I H and Delgado A 2003 *Phys. Rev. A* **68** 062316.
- [10] Kaluzny Y, Goy P, Gross M, Raimond J M and Haroche S 1983 *Phys. Rev. Lett.* **51** 1175; Rempe G, Walther H and Klein N 1987 *Phys. Rev. Lett.* **57** 353.
- [11] Boca A, Miller R, Birnbaum K M, Boozer A D, McKeever J and Kimble H J 2004 *Phys. Rev. Lett.* **93** 233603.
- [12] Eberly J H, Narozhny N B and Sanchez-Mondragon J J 1980 *Phys. Rev. Lett.* **44** 1323; Narozhny N B, Sanchez-Mondragon J J and Eberly J H 1981 *Phys. Rev. A* **23** 236; Yoo H I, Sanchez-Mondragon J J and Eberly J H 1981 *J. Phys. A* **14** 1383; Yoo H I and Eberly J H 1981 *Phys. Rep.* **118** 239.
- [13] Gea-Banacloche J 1991 *Phys. Rev. A* **44** 5913; Bužek V, Moya-Cessa H and Knight P L 1992 *Phys. Rev. A* **45** 8190; Bužek V and Hladký 1993 *J. Mod. Opt.* **40** 1309; Zaheer K and Wahiddin M R B 1994 *J. Mod. Opt.* **41** 151.
- [14] Faisal A A El-Orany and Obada A-S 2003 *J. Opt. B: Quant. Simeclass. Opt.* **5** 60.
- [15] Bose S, Fuentes-Guridi I, Knight P L and Vedral V 2001 *Phys. Rev. Lett.* **87** 050401; Ibid 279901.
- [16] Barnett S M and Knight P L 1986 *Phys. Rev. A* **22** 2444; Sharma M P, Cardimona D A and Gavrielides A 1989 *Opt. Commun.* **72** 291; Cardimona D A 1990 *Phys. Rev. A* **41** 5016; Abdalla M S, Ahmed M M A and Obada A-S F 1990 *Physica A* **162** 215, and references therein.
- [17] Iqbal M S, Mahmood S, Razmi M S K and Zubairy M S 1988 *J. Opt. Soc. Am. B* **5** 1312.
- [18] Sharma M P, Cardimona D A and Gavrielides A 1989 *J. Opt. Soc. Am. B* **6** 1942.
- [19] Jex I, Matsuoko M and Koashi M 1993 *Quant. Opt.* **5** 275
- [20] Jex I 1990 *Quant. Opt.* **2** 443
- [21] Abdel-Aty M 2004 *J. Opt. B: Quant. Semiclass. Opt.* **6** 201.
- [22] Xu L, Zhang Z-M and Chai J-L 1991 *J. Opt. Soc. Am. B* **8** 1157.
- [23] Oliveira F A M, Kim M S, Knight P L and Bužek V 1990 *Phys. Rev. A* **41** 2645.
- [24] Oliveira G C D, Almeida A R D, Queirós I P D, Moraes A M and Dantas C M A 2005 *Phys. A* **351** 251.
- [25] Moya-Cessa H 1995 *J. Mod. Opt.* **42** 1741; Dantas C M A, Queiroz J R and Baseia B 1998 *J. Mod. Opt.* **45** 1085.
- [26] Vogel K, Akulin V M and Schleich W P 1993 *Phys. Rev. Lett.* **71** 1816; Parkins A S, Marte P, Zoller P, Carnal O and Kimble H J 1995 *Phys. Rev. A* **51** 1578.
- [27] Dodonov V V and L A de Souza 2005 *J. Opt. B: Quant. Semiclass. Opt.* **7** S490.
- [28] Obada A-S F and Abd Al-Kader G M 1999 *J. Mod. Opt.* **46** 263; Faisal A A El-Orany 1999 *Czech. J. Phys. B* **49** 1145; Faisal A A El-Orany, Peřina J and Abdalla M S 1999 *J. Mod. Opt.* **46** 1621; Kamli A and Bougouffa S 2005 *Act. Phys. Hung. B* **23** 1.
- [29] Kim M S and Agarwal G S 1999 *J. Mod. Opt.* **46** 2111.

- [30] Meunier T, Gleyzes S, Maioli P, Auffeves A, Nogues G, Brune M, Raimond J M and Haroche S 2005 *Phys. Rev. Lett.* **94** 010401.
- [31] Faisal A A El-Orany 2004 *J. Phys. A: Math. Gen.* **37** 6157; Faisal A A El-Orany 2005 *J. Phys. A: Math. Gen.* **38** 5557; Faisal A A El-Orany 2005 *J. Opt. B: Quant. Semiclass. Opt.* **6** 432; Faisal A A El-Orany 2005 *J. Mod. Opt.* (submitted); Faisal A A El-Orany 2005 *J. Phys. B: At., Mol., Opt.* (submitted); Faisal A A El-Orany 2005 *Opt. Commun.* (submitted).
- [32] Faisal A A El-Orany 2004 *J. Phys. A: Math. Gen.* **37** 9037.
- [33] Eiselt J and Risken H 1989 *Opt. Commun.* **72** 351.
- [34] Eiselt J and Risken H 1991 *Phys. Rev. A* **43** 346.
- [35] Eiselt J and Risken H 1991 *Phys. Rev. A* **44** 4623; Werner M J and Risken H 1991 *Quant. Opt.* **3** 185.
- [36] Miller C A, Hilsenbeck J and Risken H 1992 *Phys. Rev. A* **46** 4323.
- [37] Faisal A A El-Orany 2002 *Phys. Rev. A* **65** 043814.
- [38] Faisal A A El-Orany, Peřina J and Abdalla M S 2000 *J. Opt. B: Quant. Semiclass. Opt.* **2** 545.
- [39] Pegg D T and Barnett S M 1988 *Europhys. Lett.* **6** 483; Ibid 1989 *Phys. Rev. A* **39** 1665; Barnett S M and Pegg D T 1989 *J. Mod. Opt.* **36** 7.
- [40] Faisal A A El-Orany, Mahran M H, Wahiddin M R B and Hashim A M 2004 *Opt. Commun.* **240** 169.
- [41] Bouwmeester D, Ekert A and Zeillinger A 2000 "The physics of quantum information" (Springer, Berlin).
- [42] Rekdal P K, Skagerstam B-S K and Knight P L 2004 *J. Mod. Opt.* **51** 75.